International Journal of GEOMATE, April, 2022, Vol.22, Issue 92, pp.1-8
ISSN: 2186-2982 (P), 2186-2990 (O), Japan, DOI: https://doi.org/10.21660/2022.92.1673
Geotechnique, Construction Materials and Environment

NUMERICAL ANALYSIS OF THE AXIAL AND RADIAL SWELLING OF UNSATURATED COMPACTED BENTONITE

*Shinya Tachibana[1], Daisuke Hayashi[2], Tomoko Ishii[2], Tomohide Takeyama[3], and Atsushi Iizuka[1]

[1]Research Center for Urban Safety and Security, Kobe University, Japan; [2]Radioactive Waste Management Funding and Research Center, Japan; [3]Graduate School of Engineering, Kobe University, Japan

*Corresponding Author, Received: 30 Nov. 2021, Revised: 01 Feb. 2022, Accepted: 23 Feb. 2022

ABSTRACT: This study deals with the problem of axial and radial swelling of a cylindrical bentonite specimen with a gap at the top or side. Unsaturated soil water coupled finite element analyses are carried out to analyze how the bentonite specimen changes during the process of swelling due to water absorption from the surface facing the gap. The behavior of the bentonite after the finite gap is filled by the swollen bentonite until the equilibrium state is also analytically evaluated. The analysis results show that the distribution of void ratio and swelling pressure in the specimen remains non-uniform in both axial and radial swelling, even if the bentonite specimen reaches a saturated and equilibrium state. In the case of axial swelling, the radial and hoop stresses remain equal at all positions in the specimen, whereas in the case of radial swelling, an anisotropic stress state, in which even the radial and hoop stresses are different, is observed immediately after the start of water absorption, resulting in the formation of complex stress distribution in the radial direction.

Keywords: Bentonite; Swelling; Finite element Analysis; elastoplastic constitutive model

1. INTRODUCTION

Compacted bentonite is expected to be used as an engineered barrier or backfill in radioactive waste repositories and as a part of a multi-barrier system that slows the migration of radionuclides from the waste body. When blocks of compacted bentonite are installed as a buffer material and stacked around the waste body, gaps are created between the blocks or between the block and the surrounding host rock or waste body. Although such gaps, referred to as "technological voids", can become water channels allowing groundwater flow if they remain intact, one of the reasons to utilize bentonite as a buffer material is that it has a sealing function to close the gaps owing to its saturation-induced swelling with groundwater infiltration.

There has been considerable interest in quantitatively understanding the state changes of bentonite originating from the presence of gaps, and several experimental efforts have been reported [1-7]. These studies have focused on the changes in the dry density distribution within the bentonite, the associated permeability of the bentonite, and the swelling pressure acting on the surfaces in contact with the bentonite, during the process of filling the gaps and afterward until the bentonite reaches equilibrium. The results of these experimental studies have shown that the average dry density of bentonite decreases during the swelling process to close the gaps. It has also been measured that this reduction generally occurs first in the vicinity of the gaps, i.e. close to the seepage surface, resulting in the formation of a non-uniform dry density distribution within the bentonite. After the gap is closed, the excess pore water pressure (or suction) gradient in the bentonite dissipates and the dry density distribution becomes more uniform, but some inhomogeneity seems to remain even after the bentonite is saturated and the mechanical equilibrium is reached. The presence of gaps has been found to affect, at the same time, the mechanism of swelling pressure generation.

In this study, finite element simulations of problems related to saturation-induced swelling and gap filling of cylindrical unsaturated compacted bentonite specimens were carried out to investigate analytically the differences in the development of non-uniform distribution of dry density and the swelling pressure depending on the swelling direction of the specimen due to the position of the gap. Two types of boundary conditions were dealt with, i.e. both axial swelling with an upper gap and radial swelling with an outer side gap. To focus on the effect of swelling direction, the initial and geometrical conditions were set so that the initial volume and initial dry density of the bentonite specimens, as well as the specimen volume and average dry density after swelling, are common.

2. ANALYSIS METHOD

The finite element code DACSAR-I [8] was used to simulate the axial and radial swelling of unsaturated compacted bentonite specimens. The code is based on the theoretical framework of unsaturated soil mechanics [9], capable of dealing with the coupling problem in which the soil deforms

under the condition where its pore is partially saturated with water. In a general unsaturated coupling problem, the fields of pore-water and pore-air pressures are approximately obtained in addition to the displacement field by simultaneously solving the spatially discretized equations for the weak form of the equilibrium equation and the continuity equations for pore water and pore air. This study, however, assumes the fully drained condition for pore air where the pore-air pressure is always equal to the atmospheric pressure everywhere in the specimen. The following sections give an overview of the material models employed in the analysis.

2.1 Elasto-Plastic Constitutive Model for Unsaturated Bentonite

The elastoplastic constitutive model for saturated bentonite proposed by Tachibana et al. [10] was extended to describe the mechanical behavior of the unsaturated state and used in the analysis. The yield surface of the model which has an elliptical shape in the effective stress space, analogous to the modified Cam-clay model [11], can be formulated as

$$f\left(p', q, p'_{\mathrm{c}}, p'_{\mathrm{s}}\right) = \frac{q^2}{\tilde{M}^2} + \left(p' - p'_{\mathrm{c}}\right)\left(p' - p'_{\mathrm{s}}\right) = 0 \quad (1)$$

Where is a material parameter determining the ellipticity of yield surface, p' is effective mean stress ($= \mathrm{tr}\boldsymbol{\sigma}'/3$), q is a stress deviator ($= \sqrt{3/2}\,\|\boldsymbol{s}\|$). $\boldsymbol{\sigma}'\left(= \boldsymbol{\sigma}^{net} + sS_{\mathrm{e}}\boldsymbol{1}\right)$ and $\boldsymbol{s}\left(= \boldsymbol{\sigma}' - p'\boldsymbol{1}\right)$ are the effective stress tensor and its deviatoric part, respectively, where is a net stress tensor (equivalent to the total stress in this study), s is a matric suction ($= p_{\mathrm{a}} - p_{\mathrm{w}}$; p_{a} : pore air pressure and pore water pressure), and is an effective degree of saturation ($= \left(S_{\mathrm{r}} - S_{\mathrm{r0}}\right)/\left(1 - S_{\mathrm{r0}}\right)$;: degree of saturation and: its residual value at the state where $s \to \infty$).

Adopting the idea of the model proposed by Ohno et al. [12] that the size of the yield surface depends not only on the plastic volumetric strain $\varepsilon_{\mathrm{v}}^{\mathrm{p}}$ but also on the effective degree of saturation, the following hardening law was formulated for the evolution of p'_{c} and p'_{s} :

$$p'_{\alpha} = p'_{\alpha}\left(\varepsilon_{\mathrm{v}}^{\mathrm{p}}, S_{\mathrm{e}}\right) = \overline{p}'_{\alpha}\left(\varepsilon_{\mathrm{v}}^{\mathrm{p}}\right) \times \xi_{\alpha}\left(S_{\mathrm{e}}\right);\ \alpha = \mathrm{c,s} \quad (2)$$

In Eq. (2), $\overline{p}'_{\mathrm{c}}$ and $\overline{p}'_{\mathrm{s}}$ were formulated in a form similar to the Cam-clay model to describe the plastic volume change along the normal consolidation line (NCL) and plastic rebound line (PRL) shown in Figure 1, respectively, as follows:

$$\overline{p}'_{\alpha} = \overline{p}'_{\alpha 0} \exp\left(\frac{1 + e_{\alpha 0}}{\lambda - \kappa}\varepsilon_{\mathrm{v}}^{\mathrm{p}}\right);\ \alpha = \mathrm{c,s} \quad (3)$$

Where is a compression index denoting the slope of both NCL and PRL, κ is a swelling index denoting the slope of 'elastic' swelling line, $\overline{p}'_{\mathrm{c0}}$ and are initial values of and, respectively. e_{c0} and are the reference void ratios corresponding to the NCL and the PRL, respectively.

ξ_{c} and ξ_{s} in Eq. (2) are parameters that control the expansion/shrink of the yield surface due to the contribution of the effective degree of saturation, and are formulated by the following equations, respectively:

$$\xi_{\mathrm{c}} = \exp\left[\left(\beta\left(S_{\mathrm{e}}\right) - 1\right)\ln\frac{1 + \zeta}{\theta + \zeta}\right];\ \left(\xi_{\mathrm{c}} \geq 1\right) \quad (4)$$

$$\xi_{\mathrm{s}} = \exp\left[\left(\beta\left(S_{\mathrm{e}}\right) - 1\right)\ln\frac{\zeta}{\theta + \zeta}\right];\ \left(0 < \xi_{\mathrm{s}} \leq 1\right) \quad (5)$$

Where is a material constant which determines the ratio of to, i.e? θ is also a material constant that determines the position of the elastic swelling line as shown Fig. 1. It is noted that the elastic swelling line is defined as a straight line connecting the point on NCL and PRL in space at any time. Therefore, the swelling index is naturally modeled as a function of the degree of saturation and is required to satisfy the following relation, in the combination with Eqs. (4) and (5), as

$$\kappa = \kappa\left(S_{\mathrm{e}}\right) = \overline{\kappa}/\beta\left(S_{\mathrm{e}}\right) \quad (6)$$

where the function determines the slope of the elastic swelling line depending on the effective degree of saturation. For to reduce at a fully saturated state, the function has to satisfy the conditions. In addition, β is required to monotonously increase according to the decrease since the model assumes the expansion of yield surface due to desaturation. Thus, the function β was formulated as a candidate satisfying the above-mentioned requirement in the form

$$\beta = \beta\left(S_{\mathrm{e}}\right) = \alpha\left(1 - S_{\mathrm{e}}^{\ l}\right) + 1 \quad (7)$$

Where and are input parameters; the former determines the maximum magnification ratio of yield surface at the driest state ($S_{\mathrm{e}} = 0$), while the latter controls the degree of influence on the swelling index.

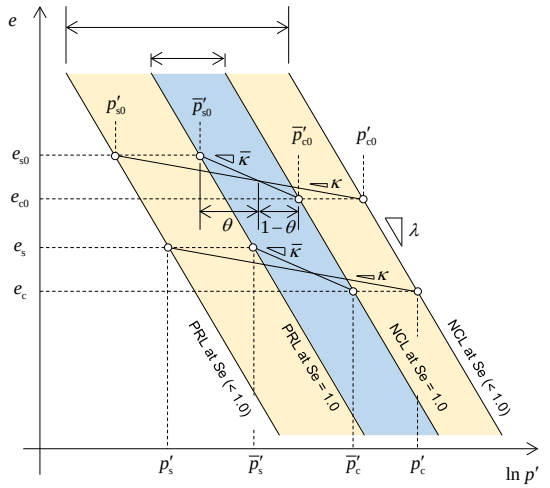

Fig. 1 Evolution of elastic region with change in saturation.

The following nonlinear elastic constitutive relationship, consistent with the elastic swelling line with the dependence of the effective degree of saturation described above, was used.

$$\dot{\boldsymbol{\sigma}}' = \boldsymbol{D}^{\mathrm{e}} : \dot{\boldsymbol{\varepsilon}}^{\mathrm{e}} - K_{\mathrm{Se}} \dot{S}_{\mathrm{e}} \boldsymbol{1} \tag{8}$$

$$\boldsymbol{D}^{\mathrm{e}} = \left(K - \frac{2}{3} G \right) \boldsymbol{1} \otimes \boldsymbol{1} + 2G\boldsymbol{I} \tag{9}$$

$$K_{\mathrm{Se}} = -\frac{1}{\beta} \frac{\partial \beta}{\partial S_{\mathrm{e}}} p' \ln \frac{(1+\zeta) p'}{(\theta+\zeta) \bar{p}'_{\mathrm{c}}} \tag{10}$$

in which the elastic bulk modulus and the shear modulus are respectively given by

$$K = \frac{1+e_{\mathrm{c0}}}{\kappa} p' \text{ and } G = \frac{3(1-2\nu')}{2(1+\nu')} K \tag{11), (12}$$

Where is Poisson's ratio?

In the elastic state, where the current stress is located inside the yield surface, Eq. (8) is used as the constitutive relation. On the other hand, in the elastoplastic state, the elastoplastic constitutive relation derived by imposing the consistency condition on the yield surface and applying the associated flow rule is used. The derivation of the constitutive relation is omitted for the sake of space, but it can be derived through a similar procedure to in the general framework of the elastoplasticity theory.

2.2 Permeability Model for Pore Water Flow

The flow of pore water is governed by Darcy's law. In this study, we simply considered only the dependence of the void ratio and adopted the following permeability model proposed by Börgesson et al. [13].

$$k = k_0 \left(e / e_0 \right)^{\lambda_{\mathrm{k}}} \tag{13}$$

Where is the hydraulic conductivity corresponding to the reference void ratio? λ_{k} is a material parameter that controls the dependence of the void ratio on the hydraulic conductivity.

2.3 Soil-Water Characteristic Curve Model

The flow of pore water is governed by Darcy's law. In this study, we simply considered only the dependence of the void ratio and adopted the following permeability model proposed by Börgesson et al. [13].

Among various models of soil-water characteristic curve (SWCC) which describe the relationship between the soil matric suction and the degree of saturation, the logistic curve model proposed by Sugii and Uno [14] was used. The curve is characterized by the following equation.

$$S_{\mathrm{r}} = S_{\mathrm{r0}} + \left(1 + S_{\mathrm{r0}}\right) \Big/ \left(1 + s^{B} \exp A\right) \tag{14}$$

Where and are material parameters that determine the shape of SWCC. Since the present study deals with a monotonically increasing response of degree of saturation, the hysteresis of soil-moisture characteristics was not considered.

3. ANALYSIS CONDITION AND INPUT PARAMETERS

The simulation was carried out by setting ideal and well-defined boundary conditions in which water infiltration and deformation occur in the either axial or radial direction of a cylindrical unsaturated compacted bentonite specimen. The mixture of Na-bentonite (Kunigel V1) and silica sand, in a proportion of 70/30 in dry mass and with a specific gravity of 2.736, was assumed to be the material to be analyzed.

Fig. 2 shows the geometric and boundary conditions for axial and radial swelling. The specimen was equally divided by 60 nine-node quadrilateral elements in the vertical direction for axial swelling and in the radial direction for radial swelling. In axial swelling, deformation in the lateral direction was constrained while the vertical deformation was allowed, but if modal points on the top surface met the gap closure condition, the displacement of those points was fixed. In other words, if the closure condition was met, the height of the specimen remained constant, while the nodal points inside the specimen could still move in the

vertical direction. On the other hand, in radial swelling, the axial deformation was constrained, while the radial deformation and the associated circumferential deformation were allowed. The displacement of the nodal points located on the side of the specimen was allowed only until the gap was closed.

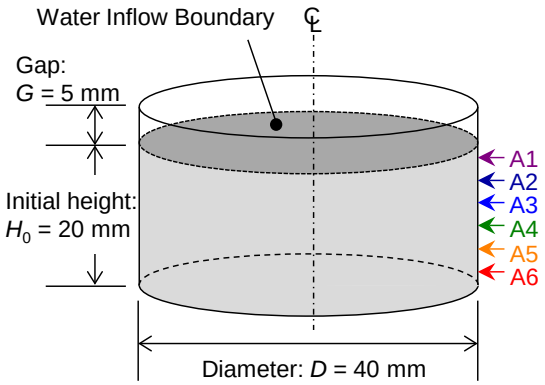

(a) Axial swelling

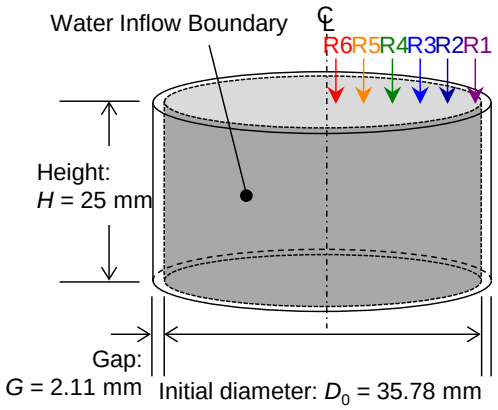

(b) Radial swelling

Fig. 2 Geometry and boundary conditions.

In both cases, the initial dry density of the bentonite specimen was set to 2.0 Mg/m^3, and the initial dimensions were set so that the swollen bentonite specimen was 25 mm high, 40 mm in diameter, and had an average dry density of 1.6 Mg/m^3 after filling the gap. The friction along the side of the specimen was not considered in the simulation. The water inflow boundary surface was set to be only on the top of the specimen for axial swelling and only on the side of the specimen for radial swelling. By setting the pore water pressure to zero on the water inflow boundary, a hydraulic gradient is formed and water infiltration is promoted as long as there is suction (negative pore water pressure) in the specimen. The state changes at the numbered locations in order of proximity from the water inflow boundary will be of interest in the next section.

Table 1 summarizes the values of the material parameters used in the analysis. Among the parameters, those related to the elastoplastic constitutive model were determined from the results of consolidation tests, undrained shear tests, and swelling pressure tests on the silica sand mixed bentonite to be analyzed. The parameters related to hydraulic conductivity and SWCC were also determined from the results of hydraulic conductivity and water retention tests on the materials, respectively.

The initial condition of the bentonite specimens is summarized in Table 2. The specimen was initially uniform and its stress state was assumed to be isotropic. The initial value of suction was determined based on SWCC, corresponding to the initial value of the degree of saturation. Since a stress-free initial stress state was assumed ($p = p^{net} = 0$), the initial effective mean stress was calculated from the product of suction and effective degree of saturation.

Table 1 Material parameter input in the simulation

Notation and symbol	Value
Critical state parameter, $\bar{M}$	0.63
Compression index, λ	0.14
Swelling index at, $\bar{\kappa}$	0.028
Poisson's ratio, ν'	0.40
Reference void ratio on NCL, e_{c0}	0.350
Pre-consolidation pressure, $\bar{p}'_{c0}$	6.795 MPa
Plastic rebound parameter, ζ	0.45
Sizing parameter, α	6.37
Positioning parameter, θ	0.65
Se-Dependency adjustment, l	2.23
Reference void ratio for, e_0	0.368
Hydraulic conductivity at, k_0	1.18e-13 m/s
e-dependency adjustment, λ_k	2.15
Residual of, S_{r0}	0.10
SWCC parameter, A	-3.00
SWCC parameter, B	4.85

Note: Eq. (1) can be obtained by. For, the value corresponding to the suction unit MPa is shown.

Table 2 Initial condition of bentonite specimen

Notation and symbol	Value
Dry density, $\rho_{d,i}$	2.0 Mg/m^3
Void ratio, e_i	0.368
Water content, w_i	10.0 %
Degree of saturation, $S_{r,i}$	74.4 %
Matric suction, s_i	1.54 MPa
Mean total stress, p_i	0 MPa
Effective mean stress, p'_i	1.10 MPa

4. NUMERICAL RESULTS

Fig. 3 shows the evolutions of the specimen height in axial swelling and the specimen radius in radial swelling. For reference, the results of the calculation without the swelling limit are shown in dashed lines. Results show that in the case of axial swelling, a 20 mm high specimen would take about 20 days to fill a 5 mm gap, and in the case of lateral swelling, a specimen with a radius of 18 mm would take about 4 days to fill a 2 mm gap. Such a change in the specimen size appears as an accumulation of local volume changes inside the specimen. Even if the gap is closed and the specimen size remains constant, there will still be pushing and pressing within the specimen. Fig. 4 shows the change in the distribution of void ratio concerning time for both cases. In the early stage of water absorption, i.e. until gaps are filled, swelling occurs gradually from

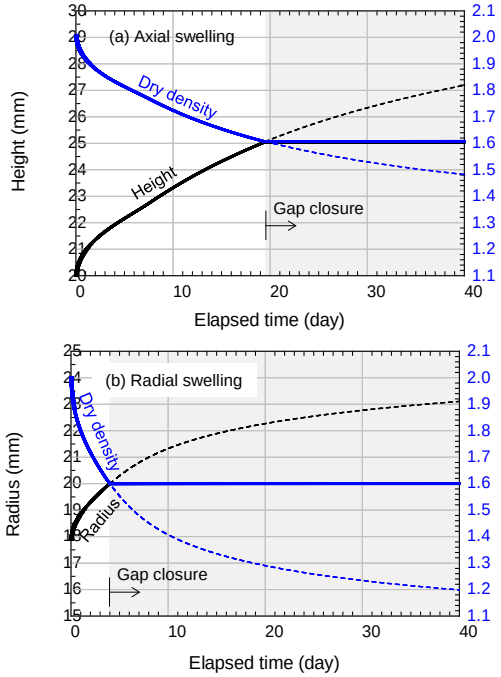

Fig. 3 Evolutions of the height/radius and the average dry density of the specimen: (a) axial swelling and (b) radial swelling.

the region close to the water inflow boundary, promoting an increase in the volume of the specimen. Once the gap is closed, the volume of the specimen remains constant, so that if there is a region of swelling, there will always be the region of shrinkage. In both axial and lateral swelling, the region farther away from the water inflow boundary swell later, causing reconsolidation in the region near the water inflow boundary. It can be seen from the figure that the void ratio distribution becomes more uniform after the gap is closed, but the distribution is not completely uniform even when the equilibrium state is reached.

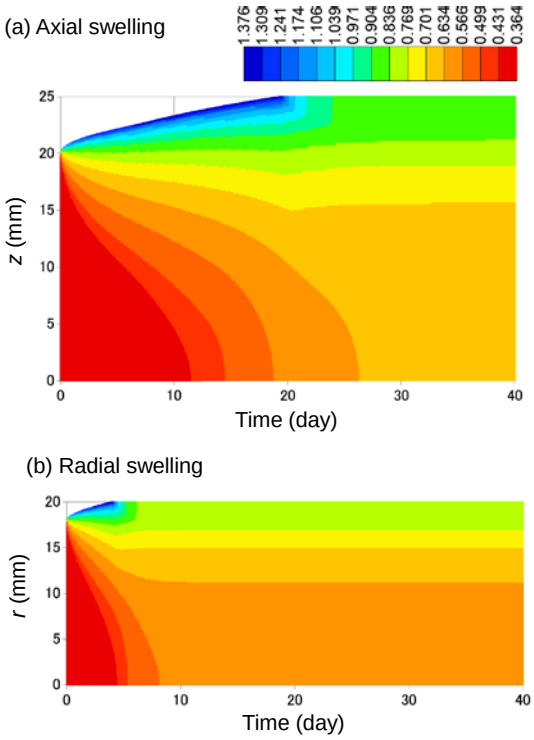

Fig. 4 Change in the distribution of void ratio in (a) axial swelling and (b) radial swelling.

The relations between void ratio and effective mean stress at 6 points in the specimen for each of the swelling problems are shown in Fig. 5. The points of interest are extracted at equal intervals in the height or radial direction of the specimen, as shown in Fig. 2, and are numbered from the side closest to the water inflow surface. Since the specimen is initially uniform, the void ratio and effective mean stress at all points are identical. The initial state is located in the elastic region bounded by the normal consolidation line and the plastic swelling line corresponding to the degree of saturation at that time on a thee-lap plane.

In the case of axial swelling, as shown in Fig. 5(a), the state change at each point follows the almost same path until the gap is closed, although there is some numerical error. In other words, under the purely axisymmetric condition where the lateral deformation is constrained and the axial stress is zero, the only axial swelling occurs as the suction decreases and the saturation increases. The farther the point is from the top surface of the specimen, the more delay there is in the response. After the gap is closed, the points at the bottom of the specimen (A4 to A6) follow the path of axial swelling with plastic deformation, while the points at the top (A1

to A3) turn to the path of reconsolidation. The reconsolidation process is elastic for a while, but there is also a region of yielding and plastic compression near the top surface, as seen from the path at point A1.

Similarly, in the case of radial swelling, swelling occurs from the side of the specimen near the water inflow boundary, and a difference in the void ratio can be seen in the specimen when the gap

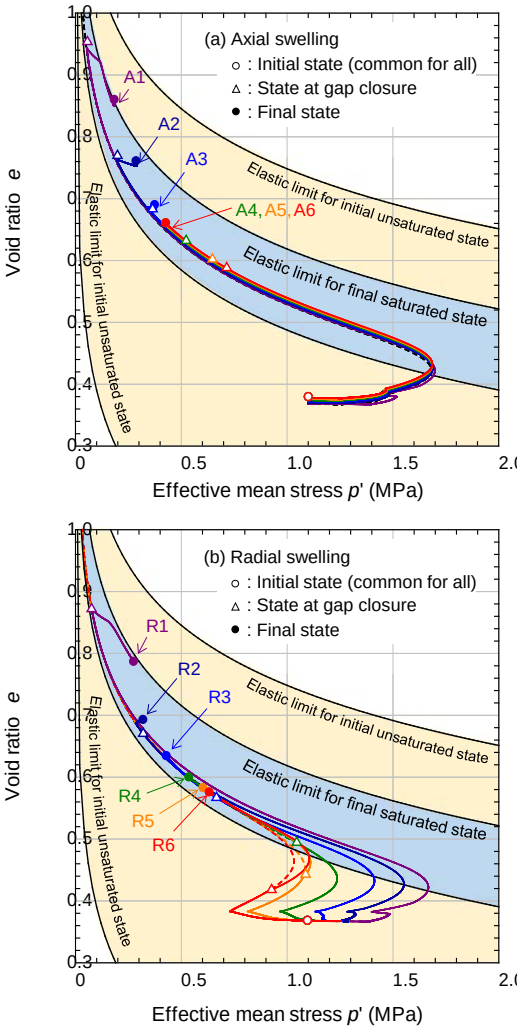

Fig. 5 State changes on the e-lnp' plane: (a) axial swelling and (b) radial swelling

is closed. On the other hand, the feature that the path differs depending on the radial position immediately after the start of water absorption is seen as a remarkable difference from axial swelling.

The swelling pressure generation in axial swelling is shown in Fig. 6. Due to the equilibrium of the axial forces in the specimen, the axial stress (σ_a : black line) is always the same at all positions along the axial axis. During the process of free swelling, until the gap is closed, the axial stress is always kept at zero. On the other hand, the radial stress increases with saturation even during the free swelling process, reaches a peak of about 1.3 MPa, and then turns to decrease. As seen in Figure 5(a), until the gap closes, the response at all points is the same with only a time delay, but the farther from the water inflow surface, the slower the infiltration speed becomes, and the slower the change in radial stress occurs. After a further time, when the gap is closed, the axial stress finally starts to increase. The calculation result shows that the axial stress increases monotonically and eventually reaches an equilibrium value of about 0.2 MPa. The radial stress also starts to monotonically increase again after the gap is closed, but the amount of increase depends on the position in the specimen. In other words, the increase is larger at the top, where reconsolidation occurs, and smaller at the bottom, where continuous swelling occurs. The equilibrium values of the radial stress also differ in the axial direction of the specimen, as does the void ratio distribution, with smaller values closer to the water inflow surface. The only point in the specimen where the equilibrium values of axial and radial stresses are equal is the isotropic stress state.

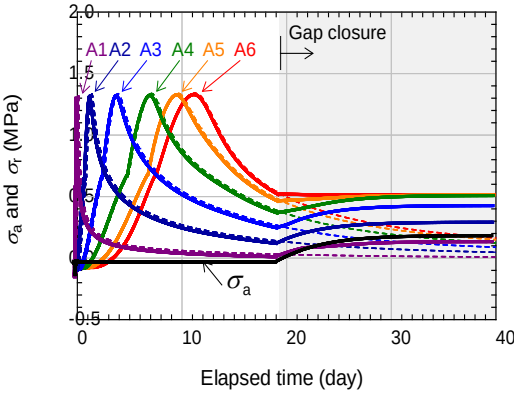

Fig. 6 Generation of swelling pressure along the axial direction in axial swelling

Fig. 7 shows the generation of swelling pressure along the radial direction in the radial swelling. In this case, even before the gap is closed, there is not only a time delay but also a difference in the magnitude of each stress component generated depending on the radial position. The R1 point closest to the water inflow boundary shows a similar response to axial swelling. In other words, the radial stress normal to the water inflow surface is zero, while the axial and hoop stresses (σ_a and σ_θ) orthogonal to are almost equal and increase rapidly immediately after the start of water absorption, reach a peak, and then decrease. On the other hand, the responses inside the specimen are that all stress components decrease once the water

absorption starts and then increase around the time the degree of saturation increases. The closer to the center of the specimen where the increase in the degree of saturation is delayed, the more pronounced the initial decrease in stress is. As time passes, if free swelling continues (see dashed lines), the radial stress at any position approaches zero from negative, while the axial and hoop stresses reach a positive peak and then decrease and approach zero. It can be seen that this peak value is larger the closer to the outside of the specimen.

After closing the gap, the axial and radial stresses converge to larger values the closer the

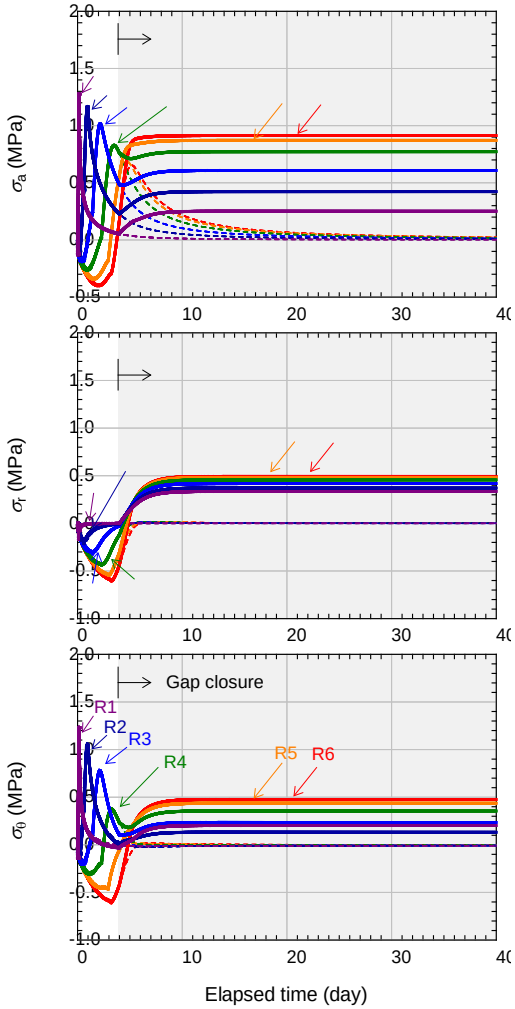

Fig. 7 Generation of swelling pressure along the radial direction in radial swelling

position is to the central axis. On the other hand, the residual value of the hoop stress is still the largest at the position close to the central axis (R6), but it is the smallest at the position slightly inside the side of the specimen (R2). In the equilibrium state, the stress state is at position R1 and at position R6, which means the maximum and intermediate principal stresses seem to differ according to the radial position.

5. CONCLUSION

This study investigates analytically the differences in the development of non-uniform distribution of dry density and the swelling pressure in each direction depending on the swelling direction of the specimen due to the position of the gap, i.e. limited axial and radial swelling. For both axial and radial swelling, the analysis results show that the non-uniform distribution of dry density (or void ratio) in the specimen formed during the gap-filling process becomes more uniform during the process of equilibrium after gap closure, but does not reach a perfect uniform distribution in both cases. The mechanism of generation of the swelling pressure orthogonal to the swelling direction differed between axial and radial swelling already in the swelling process before the gap was closed. This seems to be related to the fact that in axial swelling the axisymmetric stress condition is maintained, i.e. the two principal stresses other than the axial stress are of the same value, whereas in radial swelling the three principal stresses are different from each other. The swelling pressure at the equilibrium state after the gap is closed is also non-uniform, and the radial swelling shows not only the non-uniform distribution of axial stress in the radial direction but also the non-uniform distribution of radial and hoop stresses. As the degree of non-uniformity may vary depending on the initial and boundary conditions of the bentonite specimen, more comparisons and investigations are further needed.

6. ACKNOWLEDGMENTS

This study was conducted in “The project for validating near-field system assessment methodology in geological disposal system (FY2020)” under contract with the Ministry of Economy, Trade, and Industry of Japan (Grant Number: JPJ007597).

7. REFERENCES

[1] Komine H., Self-sealing capacity of some bentonite buffers in artificial seawater, In Procs. of the 17th Int. Conf. on Soil Mechanics and Geotechnical Engineering, 2009, pp. 2495-2498.
[2] Gens A., Valleján B., Sánchez M., Imbert C., Villar M. V., Van Geet M., Hydromechanical behavior of a heterogeneous compacted soil: experimental observations and modeling, Géotechnique, Vol. 61 (5), 2011, pp. 367-386.
[3] Dueck A., Goudarzi R., Börgesson L., Buffer homoginization, status report 3. Technical Report TR-14-25. Swedish Nuclear Fuel and Waste Management Co., 2016.
[4] Wang Q., Tang A. M., Cui Y., Delage P.,

Barnichon J, Ye W., The effects of technological voids on the hydro-mechanical behavior of compacted bentonite-sand mixture, Soils and Foundations, Vol. 53, Issue 2, 2013, pp. 232-245.
[5] Bian X., Cui Y. J., Li X. Z., Voids effect on the swelling behavior of compacted bentonite, Géotechnique, Vol. 69, (7), 2019, pp. 593-605.
[6] Jia L. Y., Chen Y. G. Ye W. M., Cui Y. J., Effects of a simulated gap on anisotropic swelling pressure of compacted GMZ bentonite, Engineering Geology, Vol. 248, 2019, pp. 155-163.
[7] Watanabe Y., Yokoyama S., Self-sealing behavior of compacted bentonite-sand mixtures containing technological voids, Geomechanics for Energy and the Environment, Vol. 25, 2021, 100213.
[8] Takeyama T., Tachibana S., Furukawa A., A finite element method to describe the cyclic behavior of saturated soil, Int. J. of Mater. Science and Engineering, Vol. 2, Issue. 1, 2015, pp. 20-25.
[9] Iizuka A., Tachibana S., Takeyama T., Sugiyama Y., Nomura S., Ohta H., Extension of unsaturated soil mechanics and its applications, Geotech. Research, Vol. 6, Issue. GR3, 2019, pp. 156-176.
[10] Tachibana S., Ito S., Iizuka A., Constitutive model with a concept of plastic rebound for expansive soil, Soils and Foundations, Vol. 60, 2020, pp. 179-197.
[11] Roscoe K. H., Burland J. H., On the generalized stress-strain behavior of 'wet' clay, In Engineering Plasticity, Cambridge Univ. Press, 1968, pp. 535-609.
[12] Ohno S., Kawai K., Tachibana S., an elastoplastic constitutive model for unsaturated soil-applied effective degree of saturation as a parameter expressing stiffness, J. JSCE, Vol. 63, Issue. 4, 2007, pp. 1132-1141. (in Japanese)
[13] Börgesson L., Johannesson L. E., Sanden T., Hernelind J., Modeling of the physical behavior of water-saturated clay barriers. Laboratory tests, material models and finite element applications, Technical Report TR-95-20. Swedish Nuclear Fuel and Waste Management Co., 1995.
[14] Sugii Y., Uno T, Modeling of hydraulic properties for unsaturated soils, Proc. Symp. Permeability of Unsaturated Ground, 1996, pp. 179-184. (in Japanese)